fire

MDPI

Article

Evaluating Landsat- and Sentinel-2-Derived Burn Indices to Map Burn Scars in Chyulu Hills, Kenya

Mary C. Henry * and John K. Maingi

Department of Geography, Miami University, Oxford, OH 45056, USA; maingijk@miamioh.edu
* Correspondence: mary.henry@miamioh.edu; Tel.: +1-513-529-5014

Abstract: Chyulu Hills, Kenya, serves as one of the region's water towers by supplying groundwater to surrounding streams and springs in southern Kenya. In a semiarid region, this water is crucial to the survival of local people, farms, and wildlife. The Chyulu Hills is also very prone to fires, and large areas of the range burn each year during the dry season. Currently, there are no detailed fire records or burn scar maps to track the burn history. Mapping burn scars using remote sensing is a cost-effective approach to monitor fire activity over time. However, it is not clear whether spectral burn indices developed elsewhere can be directly applied here when Chyulu Hills contains mostly grassland and bushland vegetation. Additionally, burn scars are usually no longer detectable after an intervening rainy season. In this study, we calculated the Differenced Normalized Burn Ratio (dNBR) and two versions of the Relative Differenced Normalized Burn Ratio (RdNBR) using Landsat Operational Land Imager (OLI) and Sentinel-2 MultiSpectral Instrument (MSI) data to determine which index, threshold values, instrument, and Sentinel near-infrared (NIR) band work best to map burn scars in Chyulu Hills, Kenya. The results indicate that the Relative Differenced Normalized Burn Ratio from Landsat OLI had the highest accuracy for mapping burn scars while also minimizing false positives (commission error). While mapping burn scars, it became clear that adjusting the threshold value for an index resulted in tradeoffs between false positives and false negatives. While none were perfect, this is an important consideration going forward. Given the length of the Landsat archive, there is potential to expand this work to additional years.

Keywords: East Africa; tropical dry forest; semiarid; grassland; bushland; burned area; dNBR; RdNBR

Citation: Henry, M.C.; Maingi, J.K. Evaluating Landsat- and Sentinel-2-Derived Burn Indices to Map Burn Scars in Chyulu Hills, Kenya. *Fire* **2024**, *7*, 472. https://doi.org/10.3390/fire7120472

Academic Editor: Aziz Ballouche

Received: 6 November 2024
Revised: 2 December 2024
Accepted: 6 December 2024
Published: 11 December 2024

1. Introduction

The arid and semi-arid lands of Kenya (commonly referred to as ASALs) make up 89% of the country's landmass, with 62% and 27% of the country falling in the arid and semi-arid categories, respectively [1]. Our study focuses on the Chyulu Hills in the semi-arid counties of Makueni, Kajiado, and Taita-Taveta in southern Kenya. Despite the Chyulu Hills being lower in elevation than some of Kenya's other water towers, it plays an important role in the region's hydrology [2]. Higher elevations in the Chyulu Hills receive greater precipitation than the surrounding areas due to orographic uplift. But this rainfall does not result in much surface runoff due to the porous volcanic rock that makes up the range [3]. Instead, much of the rainfall infiltrates to feed groundwater which, in turn, supplies nearby rivers and natural springs [4]. The Mzima Springs to the southwest is one such example, and it supplies water to the city of Mombasa 300 km away on the coast. Groundwater is also important to people who live near the Chyulu Hills, as it is a source for irrigation for local farms and water for domestic use. Water is also a critical resource for local wildlife and domestic grazing animals.

Fires have a long history in the Chyulu Hills [5], especially between June and October during the dry season following "long rains" [6]. The Chyulu Hills National Park has the highest relative frequency of fires among Kenya's protected areas [7]. Fires continue to be common due to human activities, including pasture improvement, honey harvesting, plant

growth stimulation, and clearing for improved visibility [6]. However, there are no detailed records or burn perimeter maps to assess how much of the Chyulu Hills ecosystem burns each year or which areas burn repeatedly. Climate change and increasing droughts in the region are sure to further alter fire activity in this part of Kenya.

The Chyulu Hills has a mixture of vegetation types, including grassland, wooded grassland, bushland, and forest patches (more information below). Aside from forests, the vegetation tends to recover quickly after fire, and burn scars are typically not visible after a rainy season occurs. It is clear from field photos obtained by one of the authors that even the first rain of the wet season causes grasses to begin regenerating. Given the frequency and long fire history in this landscape, satellite-based remote sensing could be a good approach to measure how much of the area burns each year.

The Differenced Normalized Burn Ratio (dNBR) [8] has become a standard method for mapping burn scars, with many researchers applying it to image data around the world [9–12]. The dNBR is calculated as the difference between pre- and post-fire Normalized Burn Ratio (NBR) images. Since it measures a change in reflectance over time to highlight burned areas, it works very well to map burn scars in a range of environments [13,14]. Researchers have applied the dNBR to map burn scars in African ecosystems, including afro-temperate forests in South Africa [15], savannas in Botswana [14], and tropical dry forests in Madagascar [13]. These studies typically collect burn severity or burned/unburned field data to calibrate dNBR to the environment they are mapping [15,16]. Other studies have used the NBR or dNBR in classification algorithms to map burn scars rather than applying direct thresholds [17,18] and found that other indices, such as the Normalized Burn Index (NBI), were more accurate for mapping burn scars in savannas in Zimbabwe.

The Relative Differenced Normalized Burn Ratio (RdNBR) was designed to measure relative change after a fire rather than absolute change, since the dNBR is correlated with pre-fire greenness [19]. A further adjustment of the RdNBR includes an offset term that is subtracted from the dNBR term in the numerator to further account for non-fire changes in greenness (e.g., phenology) between pre-fire and post-fire images [20,21]; it was found that this alternate RdNBR was more accurate than the dNBR for mapping burn severity in grasslands, woodlands, and savannas in Burkina Faso. We believe that both versions of the RdNBR might be beneficial in the Chyulu Hills, where vegetation greenness varies dramatically over the year according to wet and dry seasons. Grass-dominated vegetation types transition from high greenness during the wet season to senescent during the dry season, and a large decrease in greenness is not associated with fire. Since most fires occur during the dry season, vegetation usually loses greenness over the fire season even without being burned.

Chyulu Hills lacks systematic fire records, so it serves as a good regional test environment for using spectral burn indices to map burn scars. The biggest challenge with using remote sensing in this region is cloud cover. Even during dry seasons, there are often clouds over the landscape—especially at higher elevations. Currently, Landsat has 8-day repeat coverage using both Landsat 8 and Landsat 9 satellites, while Sentinel-2 has 5-day repeat coverage using both Sentinel 2A and Sentinel 2B satellites. Despite there being frequent coverage, there are often many consecutive weeks where cloud-free images are unavailable over the Chyulu Hills. Using image pairs from the beginning and end of the dry season might be the best approach—especially if there is some flexibility in the pre-fire image date (i.e., the pre-fire image could be from a date long before the fire season as long as it is not old enough to overlap with the previous year's fire season).

Sentinel-2 MultiSpectral Instrument (MSI) has two near-infrared NIR bands, namely the wider Band 8 (784.5–899.5 nm) at a 10 m spatial resolution and the narrower Band 8A NIR band (855–875 nm) at a 20 m resolution (Table 1). Many researchers [22,23] have used the narrower Band 8A in dNBR calculations because it is the most similar to Landsat Operational Land Imager (OLI) NIR (851–879 nm). Others have used Sentinel's wide NIR band (Band 8) [24,25] when calculating NBR-based indices. The authors of [24] conducted a study in a shrub forest-dominated landscape in northeastern Spain to evaluate the utility

of Sentinel-2 to map wildfire burns and detect burn severity. They found the Normalized Burn Ratio (NBR) for Sentinel-2 using the wider Band 8 NIR, and Band 12 SWIR emerged as the best index for delineating burned areas. Since the NBR formula only specifies the NIR in its calculation rather than a specific wavelength, we wanted to determine which Sentinel NIR band provides the most accurate results in our study area.

Table 1. Band information for Sentinel-2 MultiSpectral Instrument (MSI) and Landsat Operational Land Imager (OLI). Band names are listed as numbers with their names, central wavelength (nm), bandwidth (nm), and spatial resolution (m). Sources: [26,27].

Instrument	Band Number	Band Name	Central Wavelength (nm)	Bandwidth (nm)	Spatial Resolution (m)
Sentinel-2 MSI	1	Coastal Aerosol	443	20	60
	2	Blue	490	65	10
	3	Green	560	35	10
	4	Red	665	30	10
	5	Red Edge	705	15	20
	6	Red Edge	740	15	20
	7	Red Edge	283	20	20
	8	Near Infrared	842	115	10
	8A	Narrow Near Infrared	865	20	20
	9	Water Vapor	945	20	60
	11	Shortwave Infrared	1610	90	20
	12	Shortwave Infrared	2190	180	20
Landsat 8/9 OLI	1	Coastal Blue	443	16	30
	2	Blue	482	60	30
	3	Green	562	58	30
	4	Red	655	38	30
	5	Near Infrared	865	28	30
	6	Shortwave Infrared 1	1609	85	30
	7	Shortwave Infrared 2	2201	188	30

Our objective for this study was to evaluate methods for mapping burn scars in Chyulu Hills, Kenya. Specifically, we compared the following:

- The Differenced Normalized Burn Ratio (dNBR) and Relative Differenced Normalized Burn Ratio (RdNBR);
- A range of burn thresholds for dNBR and RdNBR;
- Landsat Operational Land Imager (OLI) and Sentintel-2 MultiSpectral Instrument (MSI) data;
- Sentinel-2 near-infrared (NIR) bands (narrow and wide).

2. Materials and Methods

2.1. Study Site

The Chyulu Hills of southern Kenya is an elongated chain of volcanic cones oriented in a northwest–southeast direction, approximately 50 km long and 10 km wide (Figure 1). The range is volcanic in origin and consists of many cinder cones and lava fields formed 260,000 years ago but had volcanic activity as recent as 700 years ago, with the last eruptions occurring in the southeastern end of the Chyulu ranges at Shetani Lava [28]. The elevation ranges from about 957 m at Kibwezi Forest to about 2055 m at the highest peak in the Chyulu National Park. High elevations receive the most rainfall due to orographic uplift (over 1000 mm), with the surrounding plains receiving around 600 mm [28]. An analysis of Climate Hazards InfraRed Precipitation with Station data version 2 (CHIRPS) for the study area for the period of 1981 to 2024 reveals annual rainfall increases from about 500 mm in the extreme northwest of the Chyulu ranges to about 950 mm in the southeastern edge. An analysis of CHIRPS data for the period of 1981 to 2024 for the protected areas (Chyulu National Park, Chyulu Conservation Area, and Kibwezi Forest) confirms the bimodal

distribution of rainfall, with a smaller peak from February to April with 246 mm received on average and a larger peak from October to December with 312 mm received. The driest period runs from June to September. This also affects fire timing so that the fire season here follows long rains rather than following short rains as it does in the Aberdares and Mount Kenya areas [29].

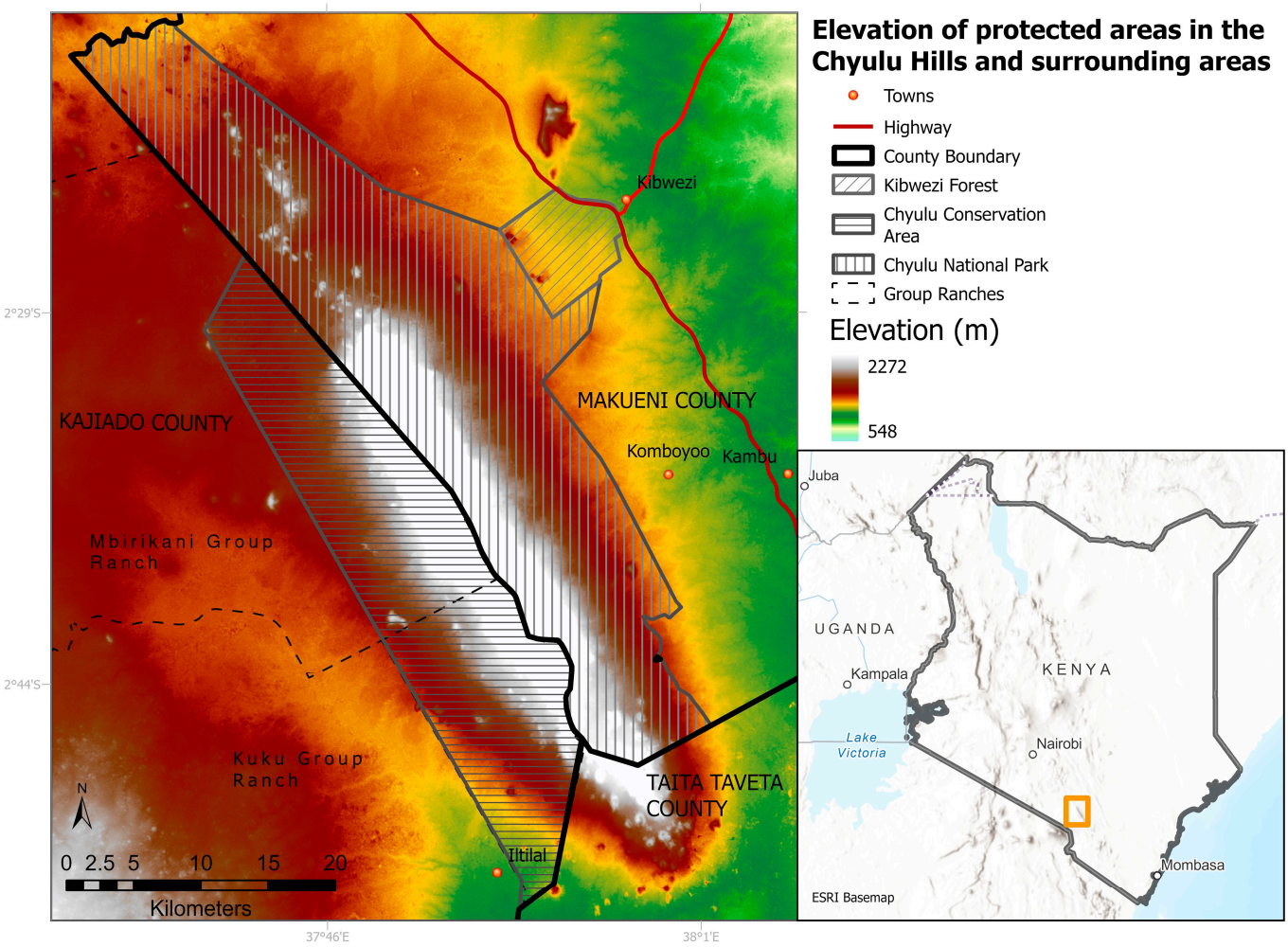

Figure 1. Location of Chyulu Hills, Kenya, in East Africa. Protected areas are shown in hatch-filled areas with labels in legend. Study area falls within three counties, Kajiado, Makueni, and Taita Taveta, as shown in map. Elevation is also shown in map, with higher elevations in white. Major roads include Mombasa Road to east of study area.

Montane or mist forest patches occur above 1800 m and consist of *Prunus africana-Ilex mitis* communities [30]. In the absence of detailed vegetation maps, we do not have specific numbers for the forest area in Chyulu Hills, but the Afromontane forests there have been described as "islands or remnant refugia" [30]. Lower elevations (1000–1600 m) contain a variety of communities, such as grasslands with scattered *Acacia drepananolobium*, *Acacia* woodlands, *Olea-Cussonia-Commiphora* bushlands in lava flow areas, and *Ozoroa/Dombeya/Combretum* woodlands. The *Juniperus* forest is found between 1300 and 1600 m, while the islands of *Erythrina abyssinica* and wooded grasslands are found at elevations of 1600 to 1800 m. Upland grassland occurs above 1600 m, while a crater forest is dominated by *Pistacia* spp., and *Vepris* spp. and *Trichocladus* spp. occur between 1300 and 1800 m. Toward the southeastern end of the Chyulu Hills range are montane forests dominated by *Drypetes* spp., *Strychnos* spp., and *Heinsenia* spp. at slightly higher elevations, and both have crater forests and southern montane forests below mist forests. Grasslands

occur at different elevations, including lower-elevation wooded grasslands and upland grasslands that occur over 1600 m [31]. The field locations used in this study are all the non-forested vegetation types, including grasslands, wooded grasslands, and bushlands.

The Chyulu Hills is managed by Kenya Wildlife Service (KWS) in Chyulu Hills National Park, local communities (Mbirikani and Kuku Group Ranches) in Chyulu Conservation Area, and Kenya Forest Service (KFS) in Kibwezi Forest. The Chyulu Hills National Park is part of the Tsavo Conservation Area (TCA), which also includes Tsavo East and Tsavo West National Parks. Past management plans for the TCA list unprescribed fire as a threat to conservation in river–lake systems, mountain forests, *Acacia-commiphora* bushlands, grasslands, and riparian habitats [32]. Fire is also identified as having unknown impacts on the forest fragments found in the Chyulu Hills [32]. Our study area was defined using the protected areas of the Chyulu Hills to ensure that most of the study area would include natural vegetation rather than agriculture and other human land uses. However, part of the protected area was excluded from both Landsat and Sentinel-2 data due to being near scene/tile edges. The area amounts to reductions of about 7500 ha from Landsat (6.2% of the study area) and 5150 ha from Sentinel-2 (4.3% of the study area).

2.2. Data

2.2.1. Satellite Image Data

Analysis procedures are summarized in Figure 2. We acquired image pairs to approximately cover the dry season for 2021 for Chyulu Hills, Kenya. These data include Landsat 8 Operational Land Imager (OLI), Landsat 9 Operational Land Imager 2 (OLI-2), Sentinel 2A and 2B, and MultiSpectral Instrument (MSI). For simplicity, we refer to OLI and OLI-2 collectively as "Landsat OLI", since the band designations are the same between them. Image dates are listed in Table 2. Level 2, Collection 2 Landsat images were downloaded from USGS EarthExplorer [33], while Sentinel-2 data were downloaded from ESA Copernicus Browser [34]. Landsat data were imported as surface reflectance images using included metadata. All bands of Collection 1, Level 2A (surface reflectance) Sentinel-2 image data were resampled to a 10-m spatial resolution using the ESA SNAP resampling tool [35]. Since Sentinel-2 data are acquired at a range of spatial resolutions, resampling all bands to 10 m allowed for a seamless analysis in ENVI 5.7 [36] and ArcGIS Pro 3.4 [37].

Table 2. A list of satellite image data used in this project. The images acquired early in the year were used as pre-fire images since they were acquired before the dry season. Images acquired later in the year were used as post-fire images since they were acquired at the end of the dry season. OLI = Operational Land Imagery; OLI2 = Operational Land Imager 2; MSI = MultiSpectral Instrument.

Instrument	Date (mm/dd/yyyy)	Timing	Processing Level	Path/Row or Tile
Landsat 8 OLI	03/03/2021	Pre-fire	Collection 2, Level 2	167/062
Landsat 9 OLI2	11/09/2021	Post-fire	Collection 2, Level 2	167/062
Sentinel 2A MSI	02/27/2021	Pre-fire	Collection 1, Level 2A	T37MCT
Sentinel 2B MSI	11/09/2021	Post-fire	Collection 1, Level 2A	T37MCT

Images were selected with the goal of minimizing cloud cover. However, all images contained at least some cloud cover. Landsat data cloud masks were created by recoding the "QA_PIXEL" band provided with the data so that all pixels corresponding to clouds or cloud shadows were assigned the value of 0, while all other pixels were assigned the value of 1. The binary cloud mask for each image in the pair was then combined to create a cloud mask that accounted for clouds and shadows on both dates, and then it was applied to the Landsat burn index images. Sentinel-2 data cloud masks were provided as binary images in the "opaque_clouds" band. The cloud masks from both dates were combined to create a combined cloud mask and applied to the Sentinel-2 burn index images.

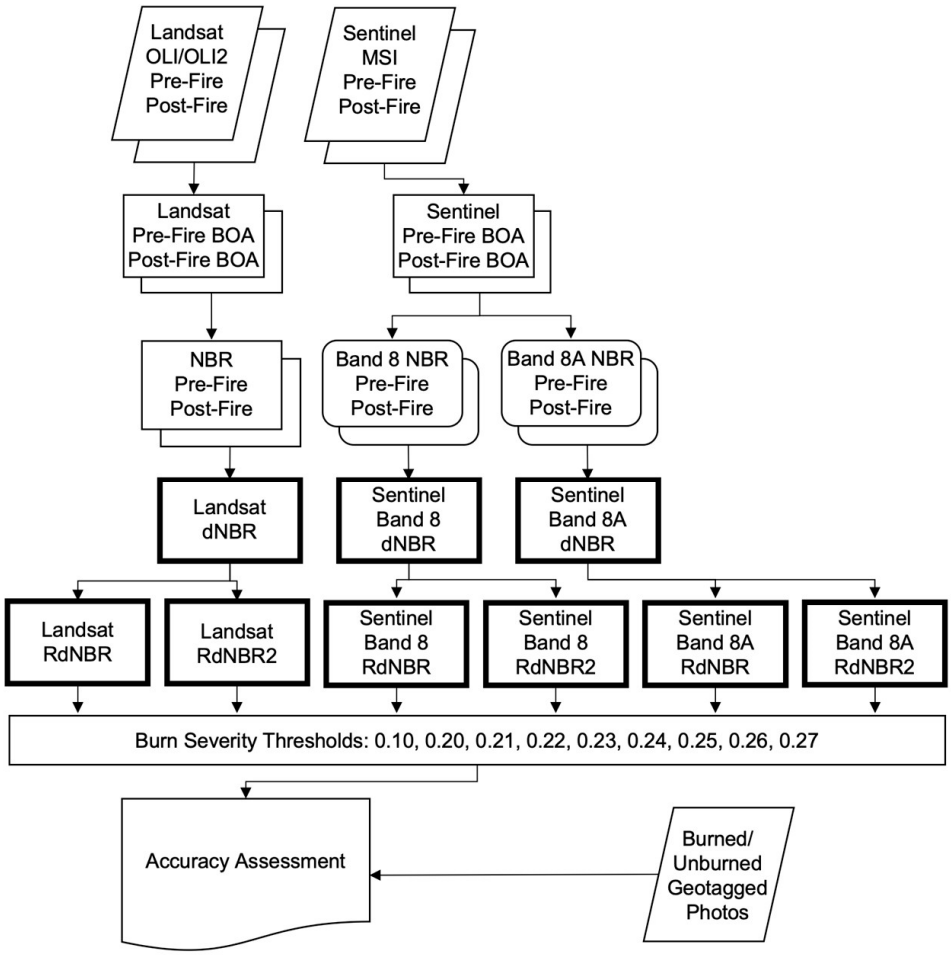

Figure 2. Flow chart showing methods used in this study. OLI = Operational Land Imager, OLI2 = Operational Land Imager 2; MSI = MultiSpectral Instrument; BOA = Bottom of Atmosphere Reflectance; NBR = Normalized Burn Ratio; dNBR = Differenced Normalized Burn Ratio; RdNBR = Relative Differenced Normalized Burn Ratio; RdNBR2 = Relative Differenced Normalized Burn Ratio alternate calculation. Boxes with bold outline indicate inputs to final analysis.

2.2.2. Field Data

On 7 and 8 October 2021, one of the authors visited several locations in the Chyulu Hills to record vegetation types and burn status by taking geotagged photos using a Garmin Montana 650 handheld GPS (spatial accuracy < 5 m [38,39]). These photos were later labeled as burned or unburned, and vegetation types were identified. Our aim was not to determine burn severity but rather to identify which locations had burned or not burned. A field assessment of burned areas would be challenging to conduct on a per-fire basis in this setting since fires are frequent and short-lived and local managers have other priorities. For this study, we visually identified burned areas by noting charred vegetation and ash, bare, blackened ground or snags during the field visit and in the photos.

Photo locations that had clouds or cloud shadows in the satellite imagery were excluded from the study to create two subsets from the original set—one set that matched cloud-free areas in both Landsat OLI scenes and one that matched cloud-free areas in both Sentinel-2 scenes. Through visual inspection, we also excluded photos that were located in the same pixel of Sentinel-2 data to avoid duplicate pixel observations (many photos were taken in clusters at the same field stop). Any photos taken of unrelated subjects or outside the study area were also removed. A total of 145 photos were used for Landsat OLI data, which were a subset of the 163 photos used for Sentinel-2 data. We used these data to extract pixel values from each burn index image for accuracy testing.

2.3. Methods

2.3.1. Satellite Image Data Processing

Each image was used to calculate the Normalized Burn Ratio (NBR) since it was an input for all other burn indices used in this study (Table 3). Each pair of NBR images was then used to calculate the dNBR: one for Landsat, one for Sentinel-2 using Band 8 (broad NIR band), and one for Sentinel-2 using Band 8A (narrow NIR band). The dNBR for each instrument was then used to calculate the RdNBR. We also calculated an alternate version of the RdNBR (hereafter referred to as RdNBR2) that includes a dNBR offset for unburned vegetation [20]. To determine the offset value, we selected 32 random points of unburned vegetation, ensuring that the points were located in protected areas. The mean unburned dNBR values were 0.3369, 0.2612, and 0.2492 for Landsat OLI, Sentinel-2 (calculated using the broad NIR band), and Sentinel-2 (calculated using the narrow NIR), respectively. In our burn index calculations, dNBR and RdNBR2 had values that typically ranged from −1 to 1, but the RdNBR values scaled with the decimal place shifted two places to the right due to the 1/1000 term in the calculation.

Table 3. Spectral burn indices used in this research. *NBR* = Normalized Burn Ratio, *NIR* = near infrared, *SWIR* = shortwave infrared, *dNBR* = Differenced Normalized Burn Ratio, $NBR_{prefire}$ = pre-fire NBR image, $NBR_{postfire}$ = post-fire NBR image, *RdNBR* = Relative Differenced Normalized Burn Ratio, *RdNBR2* = alternate calculation of Relative Differenced Normalized Burn Ratio, $dNBR_{offset}$ = average dNBR value for unburned vegetation.

Burn Index	Abbreviation	Calculation	Source
Normalized Burn Ratio	NBR	$NBR = \frac{NIR-SWIR}{NIR+SWIR}$	Key and Benson, 2006 [8]
Differenced Normalized Burn Ratio	dNBR	$dNBR = NBR_{prefire} - NBR_{postfire}$	Key and Benson, 2006 [8]
Relative Differenced Normalized Burn Ratio	RdNBR	$RdNBR = \frac{dNBR}{\sqrt{ABS\left(\frac{NBR_{prefire}}{1000}\right)}}$	Miller and Thode, 2007 [19]
Relative Differenced Normalized Burn Ratio (Alternate Calculation)	RdNBR2	$RdNBR2 = \frac{dNBR-dNBR_{offset}}{\sqrt{ABS\left(NBR_{prefire}\right)}}$	Cansler and McKenzie, 2012 [20]

The Relative Differenced Normalized Burn Ratio (RdNBR) was designed to measure relative change after a fire rather than absolute change, since dNBR is correlated with pre-fire greenness [19]. The alternate calculation of RdNBR includes an offset term to further account for non-fire changes in greenness (e.g., phenology) between pre-fire and post-fire images [20].

2.3.2. Analysis of Burn Index Images

After processing, we had nine different images to compare (listed in Table 4) from three different indices and two different satellite series (Landsat and Sentinel), and we used the broad and narrow NIR bands (8 and 8A) from Sentinel-2 data (see Figure 2).

Table 4. A list of spectral indices tested in this project and abbreviations used in the results. We tested dNBR, RdNBR, and an alternate calculation of RdNBR for Landsat, Sentinel using Band 8 for the near-infrared band, and Sentinel using Band 8A for the near-infrared band. dNBR = Differenced Normalized Burn Ratio, RdNBR = Relative Differenced Normalized Burn Ratio, RdNBR2 = alternate calculation of Relative Differenced Normalized Burn Ratio.

Burn Index	Satellite/Band	Abbreviation
dNBR	Landsat	L_dNBR
RdNBR	Landsat	L_RdNBR
RdNBR2	Landsat	L_RdNBR2

Table 4. *Cont.*

Burn Index	Satellite/Band	Abbreviation
dNBR	Sentinel-2 Band 8	S28_dNBR
RdNBR	Sentinel-2 Band 8	S28_RdNBR
RdNBR2	Sentinel-2 Band 8	S28_RdNBR2
dNBR	Sentinel-2 Band 8A	S28A_dNBR
RdNBR	Sentinel-2 Band 8A	S28A_RdNBR
RdNBR2	Sentinel-2 Band 8A	S28A_RdNBR2

2.3.3. Testing Thresholds of Burn Index Images

There are published and widely used dNBR values that are used to denote burn severity classes [8]. However, we aimed to map burned and unburned vegetation and needed to calibrate each index to the Chyulu Hills ecosystem. We used the burned and unburned classes we identified from field photos to select new thresholds for burned vegetation in dNBR, RdNBR, and RdNBR2. (Table 5). To test burned/unburned thresholds, we used values from the literature that indicate low (0.10) or moderate–low (0.27) severity. Additionally, we tested several thresholds near 0.27 since that threshold had good accuracy in initial testing.

Table 5. A list of minimum burn thresholds tested in this study. The table includes descriptions of the selection process used for each threshold value. dNBR = Differenced Normalized Burn Ratio, RdNBR = Relative Differenced Normalized Burn Ratio, RdNBR2 = alternate calculation of Relative Differenced Normalized Burn Ratio.

Threshold Tested	Description
0.10	Published minimum low-severity burn (Key and Benson, 2006) [8]
0.27	Published minimum moderate–low-severity burn (Key and Benson, 2006) [8]
0.20, 0.21, 0.22, 0.23, 0.24, 0.25, 0.26	New thresholds tested for dNBR, RdNBR, RdNBR2

For each burn threshold, we calculated overall accuracy (percent of pixels that were mapped correctly), kappa, κ (a measure of accuracy that accounts for pixels correctly mapped by chance), omission error (percent of burned pixels that were mapped as unburned), and commission error (percent of unburned pixels that were mapped as burned) for each index and satellite instrument. Omission errors can be considered false negatives, while commission error includes false positives. This resulted in a total of 81 combinations of spectral burn index, instrument or NIR band, and burn threshold values to compare (nine burn index variations x nine thresholds). We conducted a crosstabs analysis in SPSS 29.0.1.1 [40] and performed calculations for the overall accuracy, omission error, and commission error in Microsoft Excel v. 2410 [41]. We determined the best combination for the highest overall accuracy but also made comparisons between satellite instruments, burn indices, and Sentinel-2 NIR bands (Band 8 or Band 8A).

3. Results

A summary of accuracy measures is listed in Tables 6–8. For variable abbreviations, see Table 4. For simplicity, we discuss all values using the dNBR and RdNBR2 scales (e.g., 0.10). For discussion purposes, we used an 80% overall accuracy as a good value and also report omission and commission errors below 50%. These accuracies would not likely be sufficient for actually mapping burned areas but serve as a point of comparison between burn indices, satellite instruments, NIR bands, and burn threshold values.

Table 6. The accuracy of Landsat-based spectral indices for mapping burn scars. Each row shows results for a combination of spectral burn index and burn threshold value for Landsat data. dNBR = Differenced Normalized Burn Ratio, RdNBR = Relative Differenced Normalized Burn Ratio, and RdNBR2 = alternate calculation of Relative Differenced Normalized Burn Ratio. The number at the end of each index name indicates the burn threshold used (e.g., 10 = 0.10; 20 = 0.20). OE = omission error; CE = commission error.

Index	Overall Accuracy	Kappa	Burned OE (%)	Burned CE (%)
dNBR_10	30.36	0.048	0.0	75.5
dNBR_20	38.10	0.084	5.3	73.9
dNBR_21	39.29	0.093	5.3	73.5
dNBR_22	41.67	0.111	5.3	72.7
dNBR_23	42.86	0.112	7.9	72.7
dNBR_24	44.64	0.117	10.5	72.4
dNBR_25	47.02	0.137	10.5	71.4
dNBR_26	49.40	0.158	10.5	70.4
dNBR_27	52.38	0.186	10.5	69.1
RdNBR_10	35.71	0.084	0.0	74.0
RdNBR_20	83.33	0.605	7.9	41.7
RdNBR_21	85.71	0.627	18.4	35.4
RdNBR_22	90.48	0.717	26.3	17.6
RdNBR_23	91.67	0.743	28.9	10.0
RdNBR_24	90.48	0.687	39.5	4.2
RdNBR_25	87.50	0.566	52.6	5.3
RdNBR_26	86.90	0.530	57.9	0.0
RdNBR_27	85.12	0.446	65.8	0.0
RdNBR2_10	72.62	0.370	26.3	56.3
RdNBR2_20	79.76	0.422	44.7	44.7
RdNBR2_21	79.76	0.399	50.0	44.1
RdNBR2_22	79.76	0.375	55.3	43.3
RdNBR2_23	80.36	0.375	57.9	40.7
RdNBR2_24	80.36	0.375	57.9	40.7
RdNBR2_25	80.95	0.374	60.5	37.5
RdNBR2_26	84.52	0.457	60.5	16.7
RdNBR2_27	85.12	0.472	60.5	11.8

Table 7. The accuracy of Sentinel-2-based spectral indices using Band 8 for mapping burn scars. Each row shows results for a combination of a spectral burn index and burn threshold value for Sentinel data using Band 8 as the near-infrared band. dNBR = Differenced Normalized Burn Ratio, RdNBR = Relative Differenced Normalized Burn Ratio, and RdNBR2 = alternate calculation of Relative Differenced Normalized Burn Ratio. The number at the end of each index name indicates the burn threshold used (e.g., 10 = 0.10; 20 = 0.20). OE = omission error; CE = commission error.

Index	Overall Accuracy	Kappa	Burned OE (%)	Burned CE (%)
dNBR_10	32.74	0.064	0.0	74.8
dNBR_20	51.19	0.174	10.5	69.6
dNBR_21	52.98	0.182	13.2	69.2
dNBR_22	54.76	0.190	15.8	68.6
dNBR_23	57.14	0.215	15.8	67.3
dNBR_24	58.33	0.208	21.1	67.4
dNBR_25	59.52	0.221	21.1	66.7
dNBR_26	60.12	0.228	21.1	66.3
dNBR_27	62.50	0.235	26.3	65.4
RdNBR_10	36.90	0.093	0.0	73.6
RdNBR_20	79.76	0.520	15.8	46.7

Table 7. *Cont.*

Index	Overall Accuracy	Kappa	Burned OE (%)	Burned CE (%)
RdNBR_21	83.33	0.572	21.1	40.0
RdNBR_22	87.50	0.640	28.9	27.0
RdNBR_23	88.69	0.661	31.6	21.2
RdNBR_24	88.69	0.647	36.8	17.2
RdNBR_25	86.90	0.579	44.7	19.2
RdNBR_26	85.71	0.531	50.0	20.8
RdNBR_27	84.52	0.480	55.3	22.7
RdNBR2_10	70.24	0.294	36.8	60.0
RdNBR2_20	77.38	0.316	57.9	50.0
RdNBR2_21	79.76	0.363	57.9	42.9
RdNBR2_22	80.36	0.375	57.9	40.7
RdNBR2_23	80.36	0.362	60.5	40.0
RdNBR2_24	80.36	0.362	60.5	40.0
RdNBR2_25	81.55	0.387	60.5	34.8
RdNBR2_26	81.55	0.362	60.5	34.8
RdNBR2_27	82.14	0.401	60.5	31.8

Table 8. The accuracy of Sentinel-2-based spectral indices using Band 8A for mapping burn scars. Each row shows results for a combination of a spectral burn index and burn threshold value for Sentinel data using Band 8A as the near-infrared band. dNBR = Differenced Normalized Burn Ratio, RdNBR = Relative Differenced Normalized Burn Ratio, and RdNBR2 = alternate calculation of Relative Differenced Normalized Burn Ratio. The number at the end of each index name indicates the burn threshold used (e.g., 10 = 0.10; 20 = 0.20). OE = omission error; CE = commission error.

Index	Overall Accuracy	Kappa	Burned OE (%)	Burned CE (%)
dNBR_10	33.93	0.072	0.0	74.5
dNBR_20	51.19	0.156	15.8	70.4
dNBR_21	53.57	0.179	15.8	69.2
dNBR_22	55.95	0.202	15.8	68.0
dNBR_23	60.12	0.247	15.8	65.6
dNBR_24	61.31	0.241	21.1	65.5
dNBR_25	62.50	0.255	21.1	64.7
dNBR_26	63.10	0.252	23.7	64.6
dNBR_27	65.48	0.272	26.3	63.2
RdNBR_10	37.50	0.097	0.0	73.4
RdNBR_20	85.71	0.607	26.3	33.3
RdNBR_21	87.50	0.646	26.3	28.2
RdNBR_22	89.29	0.676	31.6	18.8
RdNBR_23	87.50	0.610	39.5	20.7
RdNBR_24	84.52	0.480	55.3	22.7
RdNBR_25	85.71	0.510	55.3	15.0
RdNBR_26	83.93	0.429	63.2	17.6
RdNBR_27	81.55	0.313	73.7	23.1
RdNBR2_10	71.43	0.323	34.2	58.3
RdNBR2_20	79.17	0.350	57.9	44.8
RdNBR2_21	79.76	0.363	57.9	42.9
RdNBR2_22	81.55	0.400	57.9	36.0
RdNBR2_23	82.14	0.413	57.9	33.3
RdNBR2_24	82.14	0.413	57.9	33.3
RdNBR2_25	82.14	0.401	60.5	31.8
RdNBR2_26	82.74	0.414	60.5	28.6
RdNBR2_27	84.52	0.457	60.5	16.7

3.1. Most Accurate Burn Index

Across the satellite instruments (Landsat, Sentinel-2), the RdNBR using the original calculation resulted in the highest accuracy (see Table 6). For most thresholds tested, the overall accuracies for RdNBR were over 80%. Exceptions to this were Landsat using a threshold of 0.10, Sentinel-2 Band 8 using thresholds of 0.10 and 0.20, and Sentinel-2 Band 8A using a threshold of 0.10. The fact that this index performed well across different burn thresholds and instruments indicates that it is a robust index for mapping burn scars in this environment.

Accuracy using dNBR was poor across thresholds, satellite instruments, and NIR bands ranging from 30.36% (kappa = 0.064) for Landsat using a threshold of 0.10 to 60.12% (kappa = 0.247) for Sentinel-2 Band 8A using a threshold of 0.23. The commission error for the lowest accuracy was 75.5%, and the omission error for the highest overall accuracy was 15.8%.

We expected the alternate calculation of the RdNBR (RdNBR2) to have good results given the seasonal phenology of the Chyulu Hills, and the overall accuracy ranged from 70.24% (kappa = 0.294) using Sentinel-2 Band 8 with a threshold of 0.10 to 82.14% (kappa = 0.487) using Sentinel-2 Band 8A with a threshold of 0.23. However, the commission and omission errors were often very high. The lowest accuracy had a commission error of 60.0%, and the highest accuracy had an omission error of 57.9%. There was only one combination of satellite instrument and threshold that was able to keep both omission and commission errors below 50%. Using Landsat data and a burn threshold value of 0.20 resulted in both the omission and commission errors being 44.7%. Otherwise, if the omission error was below 50%, then the commission error was greater than 50%. It appears that the offset term used in this RdNBR calculation is not beneficial for mapping burn scars in the Chyulu Hills, and the standard RdNBR works best.

3.2. Most Accurate Burn Thresholds

The highest accuracy typically resulted from using a threshold of 0.23 for RdNBR and RdNBR2, although Sentinel-2 Band 8A RdNBR2 had higher accuracy using a threshold of 0.22. Using a threshold of 0.23 with Landsat RdNBR resulted in an overall accuracy of 91.67% (kappa = 0.743). For Sentinel-2 Band 8 RdNBR, the overall accuracy was 88.69% (kappa = 0.661) for a threshold of 0.23. The overall accuracy using a threshold of 0.23 was similar for the Sentinel-2 Band 8A RdNBR, with a value of 87.50% (kappa = 0.610). Accuracy was lower when using the RdNBR2 across satellite instruments and NIR bands. Using a threshold of 0.23, Landsat RdNBR2 had an overall accuracy of 80.36% (kappa = 0.375); the Sentinel-2 Band 8 RdNBR2 had an overall accuracy of 80.36% (kappa = 0.0.661); and the Sentinel-2 Band 8A RdNBR2 had an overall accuracy of 82.14% (kappa = 0.413).

None of the overall accuracies for the dNBR were over 80% using a threshold of 0.23, although using a threshold of 0.23 for the Sentinel-2 Band 8A dNBR resulted in an overall accuracy of 60.12% (kappa = 0.247). The commission error for that test was 65.6%, so it incorrectly mapped a lot of unburned areas as burned. The trend across satellite instruments and NIR bands was that the dNBR increased in overall accuracy as the burn threshold value increased. At the same time, the omission error increased, and the commission error decreased as the burn threshold value increased. For example, with Landsat, the omission error went from 0.0% at a threshold of 0.10 to 10.5% at threshold of 0.27. For the same range, the commission error went from 75.5% at 0.10 to 69.1% at 0.27. Similar patterns were found using both NIR bands of the Sentinel-2 data as well. At low threshold values, there were extremely high commission errors, showing that almost all unburned pixels were assigned to the burned category.

3.3. Most Accurate Satellite Instrument

For the data tested here, Landsat had the highest accuracy for mapping burned areas in Chyulu Hills, Kenya. The highest overall accuracy in our tests resulted from the Landsat RdNBR using a burn threshold of 0.23 at 91.67% with a kappa of 0.743 (Table 6 and Figure 3). The omission error for this combination was 28.9%, and the commission error was 10.0%. The best results from Sentinel-2 data were obtained using the Sentinel-2 Band 8A RdNBR

using a threshold of 0.22 with an overall accuracy of 89.29% and a kappa of 0.676. The omission error was 31.6%, and the commission error was 18.8% (Table 8 and Figure 4). This Sentinel-2 result was similar to the best Landsat result, but higher errors indicate that more burned areas would be missed, and additional areas that had not actually burned would be mapped as burned. The next best Sentinel-2 accuracy was obtained with the Sentinel-2 Band 8 RdNBR using a threshold of 0.23. This resulted in an overall accuracy of 88.69% and a kappa of 0.661, but the omission error was the same at 31.6%, and the commission error was slightly higher at 21.2%.

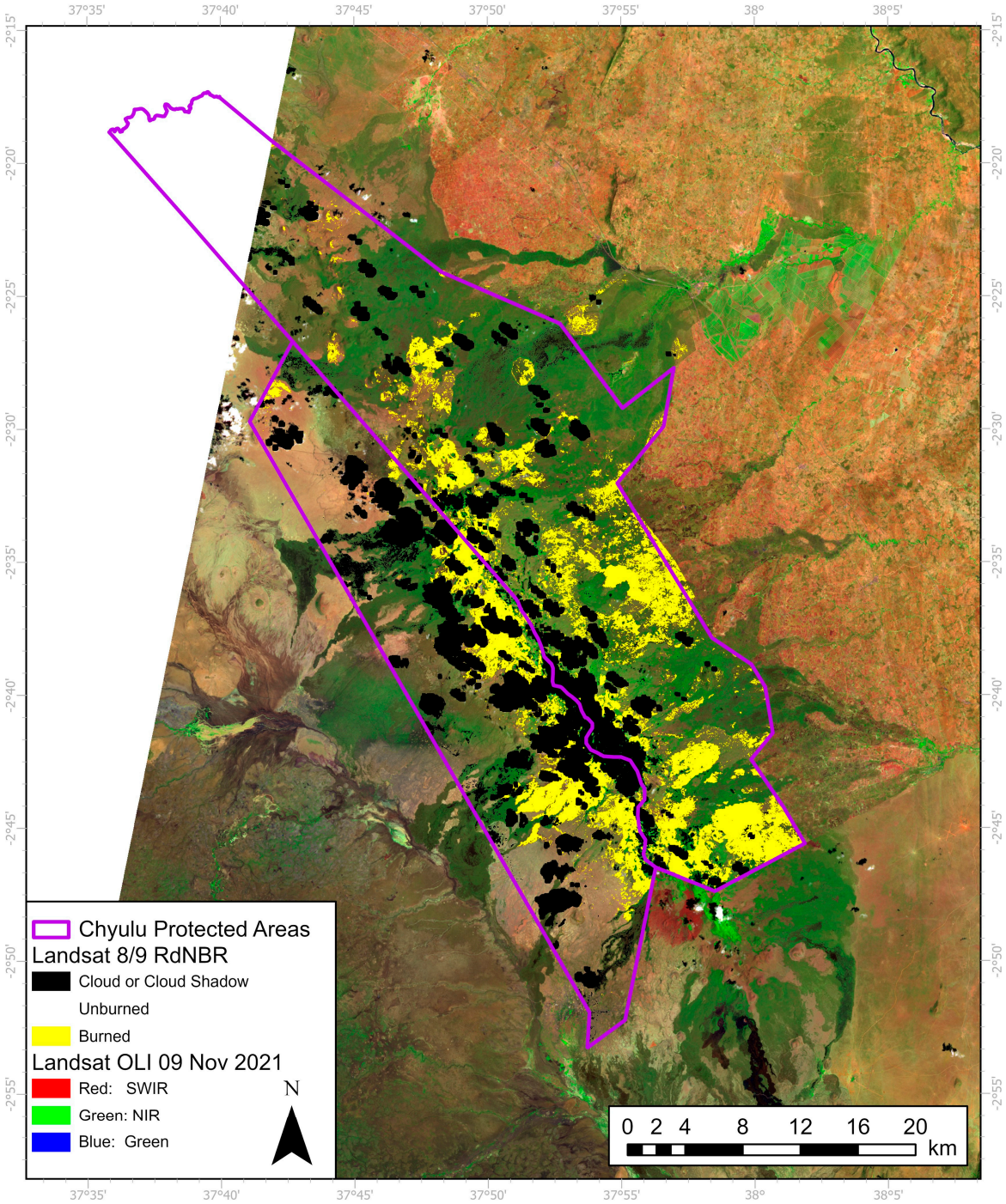

Figure 3. Mapped burn scars for the 2021 fire season in Chyulu Hills, Kenya. Yellow shows areas mapped as burned using Landsat RdNBR with a threshold of 0.23. Clouds and cloud shadows are masked out and shown in black. Purple boundaries indicate protected areas in the Chyulu Hills.

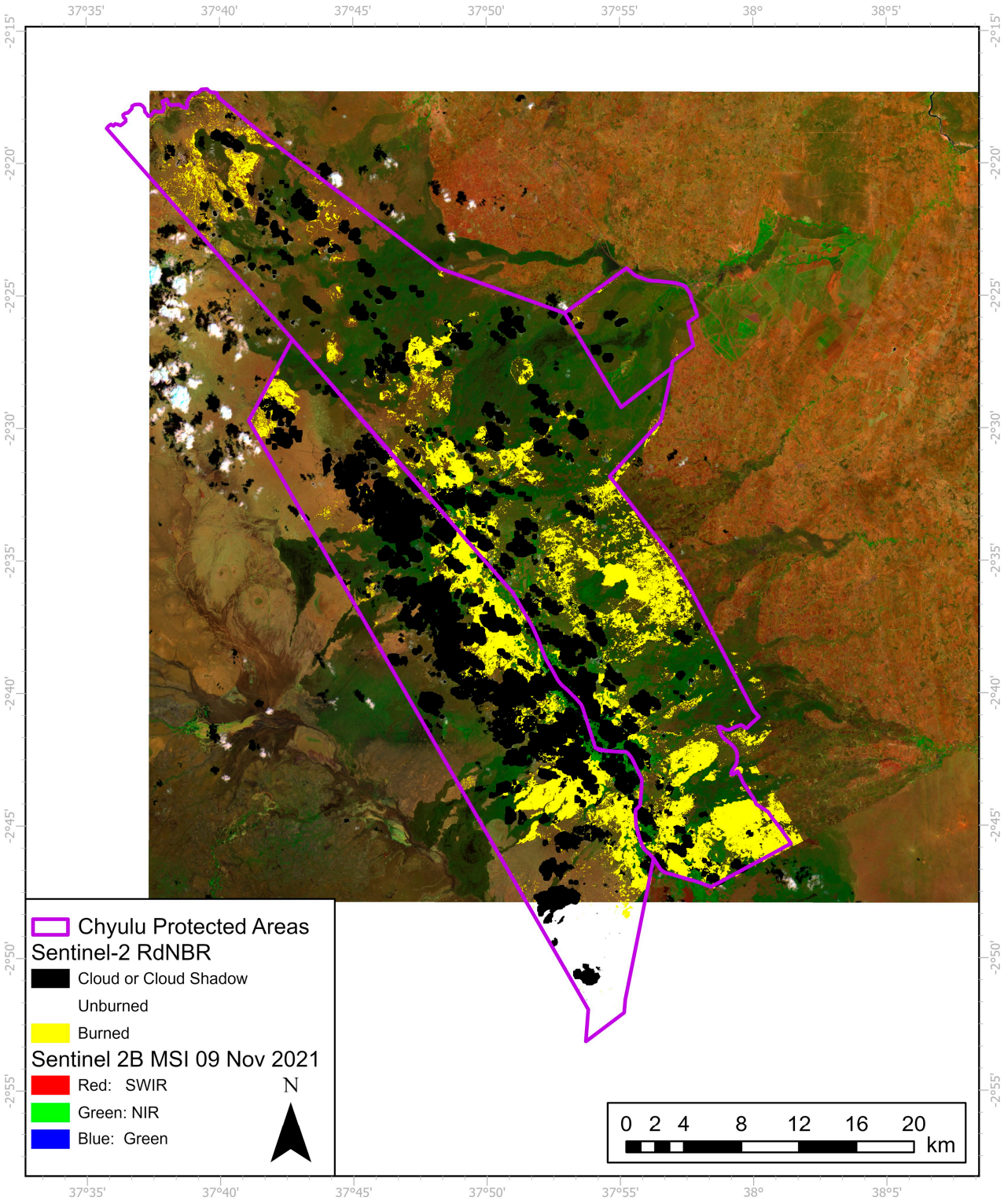

Figure 4. Mapped burn scars for the 2021 fire season in Chyulu Hills, Kenya. Yellow shows areas mapped as burned using Sentinel-2 RdNBR with a threshold of 0.22. Clouds and cloud shadows are masked out and shown in black. Purple boundaries indicate protected areas in the Chyulu Hills.

The best Landsat-based map had a burned area of 14,413 ha. The Sentinel-2-based map had a burned area of 10,750 ha. However, it is difficult to make a direct comparison between burned areas because of differences in cloud cover and the study area being cropped differently due to scene/tile characteristics. The Sentinel-2 study area was larger

at 114,374 ha (compared to Landsat's 111,708 ha), with less area masked out for clouds and cloud shadows at 13,594 ha (compared to Landsat's 17,254 ha). After subtracting the cloud-masked area from each study area size, Landsat mapped 15.26% of the study area as burned, while Sentinel-2 mapped 10.67% of the study area as burned. It seems likely that Sentinel-2 missed more burned areas, and this is indicated by the omission error of 18.8% compared to Landsat's value of 10.0%.

3.4. Most Accurate Sentinel-2 Near-Infrared Band

While the Landsat-derived RdNBR was the most accurate for mapping burn scars in the Chyulu Hills, we also compared Sentinel-2 Band 8 (wide NIR band) and Band 8A (narrow NIR band). Accuracy was similar between NIR bands, with the RdNBR with the highest overall accuracy being obtained using Band 8A and a threshold of 0.22 at 89.29% (kappa = 0.676) and using Band 8 and a threshold of 0.23 at 88.69% (kappa = 0.661). The omission error was the same for those calculations at 31.6%, with Band 8 having a slightly higher commission error of 21.2% (compared to 18.8%).

Similar patterns were found between NIR bands, with the omission error increasing as the burn threshold increased and the commission error decreasing. However, in both cases, the commission error reached its minimum at a 0.22 or 0.23 burn threshold and then increased again at 0.26 or 0.27. The omission error continued to increase as the burn threshold increased for both Band 8 and Band 8A.

4. Discussion

Our results show that the dNBR is not well suited for mapping burn scars in Chyulu Hills, Kenya. This pattern was consistent whether using Landsat or Sentinel-2 data, both Sentinel NIR bands, and across a range of burn threshold values. The seasonal changes in greenness that coincide with wet seasons in the Chyulu Hills may explain why the RdNBR is more accurate for mapping burn scars. Justification for the development of the RdNBR was the correlation between pre-fire greenness and the dNBR [19]. Published values of the dNBR were used to identify low-severity burns in Western USA forests starting at 0.10. For this study area, unburned vegetation had higher dNBR values than what would be mapped as unburned elsewhere. This is further evidenced by the dNBR offset we used to calculate the alternate RdNBR ranging from 0.2492 to 0.3369. Those were locations with unburned vegetation, but the absolute change in greenness was great due to the seasonal phenology of the vegetation. The pre-fire images we used were acquired at the end of the long rain season and were quite green in comparison to the post-fire images due to seasonal changes not related to fire. The authors of [20] listed dNBR minimum burn threshold values from studies across forests in Western North America ranging from 177 (0.177 scaled to our data) to 333 (0.333 scaled to our data). For the RdNBR, the minimum values were higher (316 to 371 or 0.316 to 0.371) [20]. Our threshold of 0.23 (230 to match their scale) falls within the ranges they list despite there being a difference in vegetation types.

One pattern we consistently found across satellite instruments and burn indices was a trade-off between omission and commission errors. In the most extreme cases, this led to some burn thresholds mapping all of our field points as burned, when only 38 out of 168 points were actually identified as burned in the field. When applying these methods to additional data in the Chyulu Hills, the trade-offs between false positives and false negatives should be considered. There might be contexts when managers would prefer to "miss" some burned areas rather than falsely identifying unburned areas as burned. Lava flows of the Chyulu Hills that make up over 12% of the study area consist of black boulders and stone outcrops and complicate the mapping of burn scars because of their similar spectral characteristics. One has to be careful not to over-map burn areas because of this. But there could also be cases where any location that had possibly burned should be identified.

Locations with the most apparent false positives were nearby agricultural fields outside the study area. These were not the focus of our study specifically, but many agricultural

fields were mapped as burn scars in our initial results. Local farmers use fire to prepare soil and clear crop residue, and some small active fires can be seen in the post-fire images (both Landsat and Sentinel-2). However, we were not able to verify fires in those areas using Visible Infrared Imaging Radiometer Suite (VIIRS) active fire detection [42]. The agricultural fields are small relative to VIIRS's 375 m spatial resolution, so it is possible that they were not detected for that reason. Fires from agricultural burning are also likely more short-lived than wildfires.

It is likely that our mapping missed or underestimated the size of other burn scars from fires earlier in the dry season. Almost all fires detected by VIIRS hotspot data in the Chyulu Hills burned between August and November 2021. One burn scar that was flagged as a hotspot by VIIRS in August already showed vegetation regrowth in the early-November images used in our analysis. Short rains usually begin in October or November, so it is likely that precipitation had caused grassland regeneration before our post-fire images were acquired.

Even with our best results, there were some burned areas missed by the Landsat RdNBR. These included some locations on the edges of lava flows and the edges of places that had burned quite recently. There is one particular burn scar visible in the post-fire image data, and when checked against VIIRS active fire detection [42], it had burned the day before post-fire image acquisition. The scar appears darker in color than older burn scars when viewed in a SWIR false color composite (OLI Band 7 shown in red, Band 5 in green, and Band 3 in blue). Yet the burn index values at the edges were just outside our threshold value of 0.23 (they were between 0.22 and 0.23). Misclassification problems at low-severity pixels are common and have been reported by different studies [10,43,44]. We did not attempt to map burn severity levels, but there would have been a range of burn effects across our study area, and low-severity burns could be spectrally similar to unburned vegetation.

These are important considerations when determining which threshold to use when mapping burn scars in the Chyulu Hills or elsewhere in Kenya. There is clearly a tradeoff between false positives (areas mapped as burned that did not burn) and false negatives (areas that burned but were mapped as unburned). Depending on the end users' goals, it might be preferable to exclude false positives or vice versa. Given that our best results for both Landsat and Sentinel-2 used burn thresholds of 0.22 and 0.23 and the accuracy levels were also good for slightly higher thresholds, we could recommend using values ranging from 0.22 to 0.25 in this setting. Using a lower threshold like 0.22 would result in more false positives, while a threshold of 0.25 would result in more false negatives. Researchers and land managers could decide which is preferable in future burn mapping.

It is interesting that Landsat had the highest accuracy for mapping burn scars in the Chyulu Hills given the coarser spatial resolution of Landsat OLI instruments compared to Sentinel-2 MSI. However, maps based on both sensors reached an acceptable level of accuracy (kappa > 0.60). The authors of [45] compared the utility of Landsat 8, Sentinel-2, and Deimos for assessing burn severity in Mediterranean fire-prone ecosystems and found that Sentinel-2 MSI only slightly improved the performance of NBR-based indices compared to Landsat 8. For our data, it appears that spatial resolution might not have been an issue given the size of most burn scars. If mapping smaller burned areas like agricultural fields, perhaps the finer spatial resolution of Sentinel-2 data would prove to be more effective. Our results agree with the findings obtained by the authors of [46] in mapping burned areas in a heterogenous savanna landscape in northwestern Zimbabwe, who found that maps derived from Landsat OLI resulted in a higher classification accuracy (kappa = 0.85) compared to those from Sentinel-2 (kappa = 0.74).

The spectral bands used in calculating the burn indices were near-infrared (NIR) and shortwave infrared (SWIR). Landsat OLI has similar wavelength ranges and bandwidths for SWIR bands when compared to Sentinel-2 MSI Band 12, but NIR bands differ between instruments (Table 1). Landsat OLI NIR (Band 5) is more similar to Sentinel-2 MSI Band 8A in wavelength range but has a wider bandwidth. Sentinel-2 MSI Band 8 has a wider

bandwidth than Band 8A or OLI NIR, but all three NIR bands have some overlap between them. It is possible that the Landsat NIR wavelength range is a good tradeoff between the two Sentinel-2 NIR bands when it comes to mapping burn scars in this setting. With respect to comparing Sentinel-2 NIR bands, the wider NIR band (8) had a higher commission error than Band 8A despite having a finer spatial resolution.

Another difference between the Landsat and Sentinel-2 data we used in this study was the image acquisition dates. The pre-fire (end of wet season) image for Landsat was acquired on 03 March 2021, while the pre-fire Sentinel-2 image was acquired on 27 February 2021—a difference of four days. It is unlikely that the slightly different acquisition dates for the Landsat OLI and Sentinel-2 pre-fire images affected the results as both periods fall right in the middle of the dry season. Both post-fire (late dry season) images were acquired on 09 November 2021 within an hour of each other. The local time at acquisition for both satellites was the late morning, so the solar angles were also similar for the images acquired near the same dates.

Spectral burn indices like the dNBR and RdNBR need to be calibrated in each new ecosystem and vegetation type where they are applied, but unburned areas in the Chyulu Hills, Kenya, had unexpectedly high values compared to other environments. One reason for this may be the prevalence of volcanic rock, soil, and lava flows that dominate the landscape in and around the Chyulu Hills. These rocks and soils are darker in color (in the visible wavelengths), so they provide a dark soil background for vegetation dominated by grasses and shrubs. During the dry season when grasses are senescent, near-infrared reflectance decreases, and shortwave infrared reflectance increases. This would lead to higher values in both the dNBR and RdNBR given how they are calculated using both wavelengths.

5. Conclusions

The results of our study show that the Landsat-based RdNBR is best for mapping burn scars in the Chyulu Hills, Kenya. When compared to the dNBR, an alternate calculation of the RdNBR (RdNBR2) and Sentinel-2 data using either NIR band, the accuracy was higher. These initial tests are a first step, but our findings suggest that it would be possible to use the same methods on additional years of image data to reconstruct fire history in the Chyulu Hills. Landsat OLI data dating back to 2013 are available, and Landsat 7 Enhanced Thematic Mapper Plus (ETM+) data are available starting from 1999; even with scan line corrector (SLC)-off data, it might be possible to map burn scars in the Chyulu Hills for those years. Despite the higher accuracy of Landsat OLI in our study, Sentinel-2 MSI data also had respectable results. Given the more frequent repeat coverage of Sentinel-2 compared to Landsat, it is still a viable option, but we would recommend using the narrow NIR band (8A) in NBR calculations.

This study focused on distinguishing burned and unburned pixels. Future studies could include a reconstruction of fire history from archived satellite imagery. The availability of detailed field data during the fire season could allow for an assessment of fire severity and resultant ecosystem effects. Persistent cloud cover remains a major hinderance to the timely mapping of wildfires and the assessment of their effects. Future studies should evaluate the utility of burn indices derived from the all-weather, all-day, and all-night Synthetic Aperture Radar (SAR) to map fire perimeters and fire severity.

Author Contributions: Both authors contributed to this manuscript. Conceptualization and Methodology, M.C.H. and J.K.M.; Formal Analysis, M.C.H.; Data Curation, M.C.H. and J.K.M.; Writing—Original Draft Preparation, M.C.H.; Writing—Review and Editing, M.C.H. and J.K.M. All authors have read and agreed to the published version of the manuscript.

Funding: This research received no external funding.

Institutional Review Board Statement: Not applicable.

Informed Consent Statement: Not applicable.

Data Availability Statement: The data are available in a publicly accessible repository. The image data used in this study are freely available to the public. Landsat data are available from the United States Geological Survey (USGS) Earth Explorer at https://earthexplorer.usgs.gov (accessed on 6 May 2024). Sentinel data are available from the European Space Agency (ESA) Copernicus Browser at https://browser.dataspace.copernicus.eu (accessed on 19 April 2024).

Acknowledgments: We would like to thank Kenya Wildlife Service for facilitating access to Chyulu Hills National Park in October 2021. We especially thank Robert Muasya for his assistance in the field and valuable insights and knowledge of the Chyulu ecosystem. We also appreciate the efforts of two anonymous reviewers whose suggestions greatly improved the quality of this manuscript.

Conflicts of Interest: The authors declare no conflicts of interest.

References

1. Government of the Republic of Kenya. *Vision 2030 Development Strategy for Northern Kenya and Other Arid Lands*; Government of the Republic of Kenya: Nairobi, Kenya, 2012.
2. Kiringe, J.W.; Mwaura, F.; Warinwa, F. Characterization of Chyulu Hills Watershed Ecosystem Services in South-Eastern Kenya. *Environ. Nat. Resour. Res.* **2016**, *6*, 65–76. [CrossRef]
3. Mwaura, F.; Kiringe, J.; Warinwa, F.; Wandera, P. Estimation of the Economic Value for the Consumptive Water Use Ecosystem Service Benefits of the Chyulu Hills Watershed, Kenya. *Int. J. Agric. For. Fish.* **2016**, *4*, 36–48.
4. Mwaura, F.; Kiringe, J.; Warinwa, F. Land Cover Dynamics in the Chyulu Watershed Ecosystem, Makueni-Kajiado Counties, Kenya. *Int. J. Agric. For. Fish.* **2016**, *4*, 17–26.
5. Spinage, C.A. *African Ecology: Benchmarks and Historical Perspectives*; Springer Geography; Springer: Berlin, Germany; New York, NY, USA, 2012; ISBN 978-3-642-22871-1.
6. Kamau, P.N.; Medley, K.E. Anthropogenic Fires and Local Livelihoods at Chyulu Hills, Kenya. *Landsc. Urban Plan.* **2014**, *124*, 76–84. [CrossRef]
7. Karanja, S.K. Density-Based Cluster Analysis of Fire Hot Spots in Kenya's Wildlife Protected Areas. Master's Thesis, University of Nairobi, Nairobi, Kenya, 2016.
8. Key, C.; Benson, N. Landscape Assessment: Ground Measure of Severity, the Composite Burn Index; and Remote Sensing of Severity, the Normalized Burn Ratio. In *FIREMON: Fire Effects Monitoring and Inventory System*; USDA Forest Service, Rocky Mountain Research Station: Ogden, UT, USA, 2006; pp. LA1–LA51.
9. Chen, X.; Vogelmann, J.E.; Rollins, M.; Ohlen, D.; Key, C.H.; Yang, L.; Huang, C.; Shi, H. Detecting Post-Fire Burn Severity and Vegetation Recovery Using Multitemporal Remote Sensing Spectral Indices and Field-Collected Composite Burn Index Data in a Ponderosa Pine Forest. *Int. J. Remote Sens.* **2011**, *32*, 7905–7927. [CrossRef]
10. Cocke, A.E.; Fulé, P.Z.; Crouse, J.E. Comparison of Burn Severity Assessments Using Differenced Normalized Burn Ratio and Ground Data. *Int. J. Wildland Fire* **2005**, *14*, 189–198. [CrossRef]
11. Fassnacht, F.E.; Schmidt-Riese, E.; Kattenborn, T.; Hernández, J. Explaining Sentinel 2-Based dNBR and RdNBR Variability with Reference Data from the Bird's Eye (UAS) Perspective. *Int. J. Appl. Earth Obs. Geoinf.* **2021**, *95*, 102262. [CrossRef]
12. Mohammad, L.; Bandyopadhyay, J.; Sk, R.; Mondal, I.; Nguyen, T.T.; Lama, G.F.C.; Anh, D.T. Estimation of Agricultural Burned Affected Area Using NDVI and dNBR Satellite-Based Empirical Models. *J. Environ. Manag.* **2023**, *343*, 118226. [CrossRef]
13. Axel, A. Burned Area Mapping of an Escaped Fire into Tropical Dry Forest in Western Madagascar Using Multi-Season Landsat OLI Data. *Remote Sens.* **2018**, *10*, 371. [CrossRef]
14. Kaduyu, I.; Tsheko, R.; Chepete, J.H.; Kgosiesele, E. *Burned Area Estimation and Severity Classification Using the Fire Mapping Tool (Fmt) in Arid Savannas of Botswana, a Case Study—Kgalagadi District*; Heliyon: Cambridge, MA, USA, 2023.
15. Giddey, B.L.; Baard, J.A.; Kraaij, T. Verification of the Differenced Normalised Burn Ratio (dNBR) as an Index of Fire Severity in Afrotemperate Forest. *S. Afr. J. Bot.* **2022**, *146*, 348–353. [CrossRef]
16. Adagbasa, G.E.; Adelabu, S.A.; Okello, T.W. Spatio-Temporal Assessment of Fire Severity in a Protected and Mountainous Ecosystem. In Proceedings of the IGARSS 2018—2018 IEEE International Geoscience and Remote Sensing Symposium, Valencia, Spain, 22–27 July 2018; pp. 6572–6575.
17. Xulu, S.; Mbatha, N.; Peerbhay, K. Burned Area Mapping over the Southern Cape Forestry Region, South Africa Using Sentinel Data within GEE Cloud Platform. *ISPRS Int. J. Geo-Inf.* **2021**, *10*, 511. [CrossRef]
18. Mpakairi, K.S.; Kadzunge, S.L.; Ndaimani, H. Testing the Utility of the Blue Spectral Region in Burned Area Mapping: Insights from Savanna Wildfires. *Remote Sens. Appl. Soc. Environ.* **2020**, *20*, 100365. [CrossRef]
19. Miller, J.D.; Thode, A.E. Quantifying Burn Severity in a Heterogeneous Landscape with a Relative Version of the Delta Normalized Burn Ratio (dNBR). *Remote Sens. Environ.* **2007**, *109*, 66–80. [CrossRef]
20. Cansler, C.A.; McKenzie, D. How Robust Are Burn Severity Indices When Applied in a New Region? Evaluation of Alternate Field-Based and Remote-Sensing Methods. *Remote Sens.* **2012**, *4*, 456–483. [CrossRef]
21. Musyimi, Z.; Said, M.Y.; Zida, D.; Rosenstock, T.S.; Udelhoven, T.; Savadogo, P.; De Leeuw, J.; Aynekulu, E. Evaluating Fire Severity in Sudanian Ecosystems of Burkina Faso Using Landsat 8 Satellite Images. *J. Arid Environ.* **2017**, *139*, 95–109. [CrossRef]

22. Zhang, H.K.; Roy, D.P.; Yan, L.; Li, Z.; Huang, H.; Vermote, E.; Skakun, S.; Roger, J.-C. Characterization of Sentinel-2A and Landsat-8 Top of Atmosphere, Surface, and Nadir BRDF Adjusted Reflectance and NDVI Differences. *Remote Sens. Environ.* **2018**, *215*, 482–494. [CrossRef]
23. Saulino, L.; Rita, A.; Migliozzi, A.; Maffei, C.; Allevato, E.; Garonna, A.P.; Saracino, A. Detecting Burn Severity across Mediterranean Forest Types by Coupling Medium-Spatial Resolution Satellite Imagery and Field Data. *Remote Sens.* **2020**, *12*, 741. [CrossRef]
24. Amos, C.; Petropoulos, G.P.; Ferentinos, K.P. Determining the Use of Sentinel-2A MSI for Wildfire Burning & Severity Detection. *Int. J. Remote Sens.* **2019**, *40*, 905–930. [CrossRef]
25. Howe, A.A.; Parks, S.A.; Harvey, B.J.; Saberi, S.J.; Lutz, J.A.; Yocom, L.L. Comparing Sentinel-2 and Landsat 8 for Burn Severity Mapping in Western North America. *Remote Sens.* **2022**, *14*, 5249. [CrossRef]
26. European Space Agency. *Sentinel-2 User Guide*; European Union: Brussels, Belgium, 2015.
27. United States Geological Survey (USGS). *Fact Sheet*; United States Geological Survey: Reston, VA, USA, 2015.
28. Wright, E.P.; Gunston, H.M. *Hydrogeology of the Chyulu Hills Basalt Aquifer, Kenya*; Institute of Hydrology: Wallingford, UK, 1988.
29. Henry, M.C.; Maingi, J.K.; McCarty, J. Fire on the Water Towers: Mapping Burn Scars on Mount Kenya Using Satellite Data to Reconstruct Recent Fire History. *Remote Sens.* **2019**, *11*, 104. [CrossRef]
30. Meguro, S.-I.; Chalo, D.; Mutiso, P. Vegetation at Arabuko-Sokoke (Kilifi County) and Chyulu Hills National Park (Makueni County), Kenya. *Eco-Habitat* **2018**, *25*, 37–50.
31. Pócs, T.; Luke, Q. East African Bryophytes, XXV: Bryological Records from the Chyulu Range, Kenya. *J. East Afr. Nat. Hist.* **2007**, *96*, 27–46. [CrossRef]
32. Kenya Wildlife Service. *Tsavo Conservation Area Management Plan 2008–2018*; Kenya Wildlife Service: Nairobi, Kenya, 2008; p. 195.
33. United States Geological Survey (USGS). Earth Explorer, Landsat Collection 2, Level 2 BOA Reflectance Product. Available online: https://earthexplorer.usgs.gov/ (accessed on 6 May 2024).
34. European Space Agency. *Sentinel-2 MSI Level-2A BOA Reflectance 2022*; European Union: Brussels, Belgium, 2023.
35. European Space Agency. *Sentinel Application Platform (SNAP)*; European Space Agency: Paris, France, 2024.
36. NV5. *Geospatail Software ENVI*; NV5 Geospatial Solutions, Inc.: Hollywood, FL, USA, 2023.
37. ESRI, Inc. *ArcGIS Pro*; Esri: Tokyo, Japan, 2024.
38. Szot, T.; Specht, C.; Dabrowski, P.S.; Specht, M. Comparative Analysis of Positioning Accuracy of Garmin Forerunner Wearable GNSS Receivers in Dynamic Testing. *Measurement* **2021**, *183*, 109846. [CrossRef]
39. Garnett, R.; Stewart, R. Comparison of GPS Units and Mobile Apple GPS Capabilities in an Urban Landscape. *Cartogr. Geogr. Inf. Sci.* **2015**, *42*, 1–8. [CrossRef]
40. IBM. *SPSS*; IBM: Armonk, NY, USA, 2024.
41. Microsoft. *Excel*; Microsoft: Redmond, WA, USA, 2024.
42. NASA FIRMS. *VIIRS (S-NPP) I Band 375 m Active Fire Locations NRT (Vector Data)*; NASA: Washington, DC, USA, 2020.
43. Sunderman, S.O.; Weisberg, P.J. Remote Sensing Approaches for Reconstructing Fire Perimeters and Burn Severity Mosaics in Desert Spring Ecosystems. *Remote Sens. Environ.* **2011**, *115*, 2384–2389. [CrossRef]
44. Stambaugh, M.; Hammer, L.; Godfrey, R. Performance of Burn-Severity Metrics and Classification in Oak Woodlands and Grasslands. *Remote Sens.* **2015**, *7*, 10501–10522. [CrossRef]
45. García-Llamas, P.; Suárez-Seoane, S.; Fernández-Guisuraga, J.M.; Fernández-García, V.; Fernández-Manso, A.; Quintano, C.; Taboada, A.; Marcos, E.; Calvo, L. Evaluation and Comparison of Landsat 8, Sentinel-2 and Deimos-1 Remote Sensing Indices for Assessing Burn Severity in Mediterranean Fire-Prone Ecosystems. *Int. J. Appl. Earth Obs. Geoinf.* **2019**, *80*, 137–144. [CrossRef]
46. Ngadze, F.; Mpakairi, K.S.; Kavhu, B.; Ndaimani, H.; Maremba, M.S. Exploring the Utility of Sentinel-2 MSI and Landsat 8 OLI in Burned Area Mapping for a Heterogenous Savannah Landscape. *PLoS ONE* **2020**, *15*, e0232962. [CrossRef]